Structural Investigations of a Human Calcitonin-Derived Carrier Peptide in a Membrane Environment by Solid-State NMR[†]

Kerstin Wagner,[‡,§] Annette G. Beck-Sickinger,[‡] and Daniel Huster*[,§]

Institute of Biochemistry, University of Leipzig, Brüderstrasse 34, D-04103 Leipzig, Germany, and Junior Research Group "Solid-state NMR Studies of the Structure of Membrane-associated Proteins", Biotechnological-Biomedical Center of the University of Leipzig, Institute of Medical Physics and Biophysics, University of Leipzig, Liebigstrasse 27, D-04103 Leipzig, Germany

Received April 23, 2004; Revised Manuscript Received July 28, 2004

ABSTRACT: Previous studies have shown that human calcitonin (hCT) and its C-terminal fragment hCT(9−32) translocate in nasal epithelium. Moreover, hCT(9−32) was used as a carrier to internalize efficiently the green fluorescent protein, drugs, and plasmid DNA. To understand the mechanism of the membrane crossing process, we determined structural parameters of the carrier peptide hCT(9−32) in a membrane environment using solid-state NMR. For that purpose, we synthesized a multiply labeled hCT(9−32) peptide comprising four positions with fully ^{15}N- and ^{13}C-labeled amino acids. Multilamellar vesicle samples containing varying mixing ratios of hCT(9−32) and phospholipids found in the plasma membrane of nasal epithelium were prepared. The typical axially symmetric powder patterns of ^{31}P NMR spectra confirmed the presence of lamellar bilayers in our samples. The chemical shift anisotropy of the ^{31}P NMR spectra of the samples in the presence of hCT(9−32) is slightly reduced, revealing weak interaction of the peptide with the lipid headgroups. The peptide does not penetrate the lipid membrane as indicated by very similar ^{2}H NMR order parameters of the phospholipid fatty acid chains in the absence and presence of the carrier peptide. This membrane topology was confirmed by measurements of paramagnetic enhancement of relaxation rates. The conformation of hCT(9−32) was investigated by cross polarization magic angle spinning NMR methods. All peptide signals were resolved and fully assigned in two-dimensional proton-driven ^{13}C spin diffusion experiments. The isotropic chemical shifts of ^{13}CO, ^{13}Cα, and ^{13}Cβ provide information about the secondary structure of the carrier peptide. The conformation of hCT(9−32) was further corroborated by quantitative ϕ torsion angle measurements. Two monomeric structural models are consistent with the data: (i) a linear backbone conformation of hCT(9−32) and (ii) an antiparallel β-sheet structure. These structures are maintained over a wide range of peptide:lipid mixing ratios. No direct indications for fibril formation of hCT(9−32) were found. Dipolar coupling measurements indicate rather high amplitudes of motion of the peptide.

Efficient drug delivery of classical pharmaceuticals and applications of modern gene and protein therapeutics are attracting more interest in both basic research and the pharmaceutical industry. The cellular uptake of peptides, proteins, oligonucleotides, or plasmid DNA is hindered by the plasma membrane representing a hydrophobic barrier against the permeation of polar molecules. To overcome this barrier, cell penetrating peptides (CPPs)[1] have been designed. These molecules are able to cross the cellular membrane, thereby facilitating the permeation of even large hydrophilic molecules as their cargoes. These CPPs, also termed carrier peptides, have evolved to become a promising tool in the transport of drugs and genes into cells (*1*−*3*). Unlike pore formation by detergents, toxins, or electroporation, carrier peptides are less toxic and very versatile in their applications. Several CPPs have been designed and applied for cellular targeting in the past years, such as penetratin (*4*), MPG (*5*), and transportan (*6*).

Membrane crossing properties have also been observed for human calcitonin (hCT) and peptides derived from its

---

[†] This work was supported by EU Grant QLK2-2001-01451 (A.G.B.-S.) and by a grant from the Deutsche Forschungsgemeinschaft (HU 720/5-1 to D.H.).

* To whom correspondence should be addressed. Telephone: +49 (0) 341-97-15706. Fax: +49 (0) 341-97-15709. E-mail: husd@medizin.uni-leipzig.de.

[‡] Institute of Biochemistry, University of Leipzig.

[§] Institute of Medical Physics and Biophysics.

[1] Abbreviations: CD, circular dichroism; CP, cross polarization; CPP, cell-penetrating peptide; DIPSHIFT, dipolar coupling and chemical shift correlation; 5-Doxyl-PC, 1-palmitoyl-2-stearoyl-(5-DOXYL)-*sn*-glycero-3-phosphocholine; FSLG, frequency-switched Lee Goldburg; hCT, human calcitonin; hCT(9−32), C-terminal fragment of hCT; HETCOR, heteronuclear correlation; HNCH, ^{1}H−^{15}N−^{13}C−^{1}H correlation experiment for ϕ torsion angle determination; LUV, large unilamellar vesicles; MALDI, matrix-assisted laser desorption ionization; MAS, magic angle spinning; MDCK, Madin-Darby canine kidney; MLV, multilamellar vesicles; PDSD, proton-driven spin diffusion; POPC, 1-palmitoyl-2-oleoyl-*sn*-glycero-3-phosphocholine; POPC-d_{31}, 1-palmitoyl-d_{31}-2-oleoyl-*sn*-glycero-3-phosphocholine; POPE, 1-palmitoyl-2-oleoyl-*sn*-glycero-3-phosphoethanolamine; POPG, 1-palmitoyl-2-oleoyl-*sn*-glycero-3-[phospho-*rac*-(1-glycerol)]; REDOR, rotational echo double resonance; rmsd, root-mean-square deviation; SDS, sodium dodecyl sulfate; Tempo-PC, 1-palmitoyl-2-oleoyl-*sn*-glycero-3-phospho-(TEMPO)choline; TFA, trifluoroacetic acid; TPPM, two-pulse phase modulation.

10.1021/bi049181y CCC: $27.50

sequence (*7*, *8*). The peptide hormone hCT is a 32-amino acid peptide that is expressed by the C-cells of the thyroid gland. The finding that intranasal therapeutic application of hCT is as effective as intravenous injection (*9*) even led to the development of an easy-to-use nasal spray (*10*). Carrier peptide properties have been observed for C-terminal fragments of hCT, in which the receptor activating N-terminus of hCT has been cleaved off (*7*, *11*). For the most efficient fragment, amino acids 9−32 [hCT(9−32)], carrier properties have been demonstrated for Madin-Darby canine kidney (MDCK) cells (*12*). Efficiently internalized cargo molecules include the green fluorescent protein (*12*), the drug Daunorubicin (*13*), and plasmid DNA (*14*).

The mechanism of cell uptake for most carrier peptides is not understood. Varying characteristic structural features argue in favor of specific internalization pathways for each of these molecules. Several peptides permeate the plasma membrane at both a physiological (37 °C) and a low temperature (4 °C), suggesting an energy-independent transport mechanism. For penetratin, for instance, peptide translocation by formation of inverse micelles (*4*) or purely electrostatic interactions ("electroporation-like internalization") are discussed (*15*).

For hCT, non-receptor-mediated internalization mechanisms have been proposed (*7*). At physiological temperature, the flux from the mucosal to serosal side is approximately twice as high as in the opposite direction. At low temperatures, the flux rate is decreased to ∼25% and no directional specificity could be observed. From this study, it was concluded that an endocytic pathway contributes to the transport of hCT across nasal epithelium at physiological temperature (*8*).

To understand the mechanism of membrane crossing, several model studies have been carried out to determine structural parameters of hCT. In the aqueous phase, hCT is largely unstructured, while at high hCT concentrations, oligomeric β-sheet structures (fibrils) have been observed (*16*−*18*). Organic solvents with low dielectric constants such as trifluoroethanol or methanol on the other hand induce α-helical structures (*18, 19*). Amphipathic helical segments (amino acids 8−22) of hCT have also been identified (*20*, *21*). These studies were corroborated by high-resolution structures determined by NMR spectroscopy in membrane-mimicking SDS micelles (*22*−*24*). In contrast, short β-sheet structures have also been observed in similar systems (*25*).

Fewer structural studies have been carried out for hCT in mucosa or phospholipid model membranes (*7, 21*, *26*). It was first found that hCT is able to deform and solubilize phosphatidylglycerol vesicles, which, in turn, induce a low helical content in hCT (*21*). Later, an intermolecular β-sheet formation has been suggested for the tail residues of hCT, which could possibly lead to membrane embedding of the C-terminus with a subsequent internalization (*7*). This shows the dependence of the structural information on the experimental system and method.

For the carrier peptide fragment hCT(9−32), so far, only one structural study has been published (*27*). From its characteristic membrane crossing properties, one would expect the peptide to penetrate lipid bi- and monolayers. However, monolayer experiments indicated that the critical pressure of insertion is on the order of 15−20 mN/m for both zwitterionic and negatively charged lipids, which is far below the value of ∼35 mN/m that is expected for cell membranes (*28*).

In this paper, we have applied solid-state NMR methods to study structure and membrane interactions of hCT(9−32) with true lipid membranes composed of a nasal epithelium-like lipid mixture. In contrast to CD or infrared spectroscopy, NMR spectroscopy can reveal site-specific structural information with high precision. However, due to the lack of fast isotropic tumbling of the membrane-associated peptides, NMR signals are broadened by dipolar couplings and the chemical shift anisotropy. These hardships can be overcome by the application of solid-state NMR methods such as magic angle spinning (MAS) in combination with dipolar decoupling (*29*). Solid-state NMR is a promising tool for studying the conformation of membrane-associated peptides (*30*−*37*). With isotopic labeling, specific sites in a peptide for which the local structure is determined can be highlighted. Therefore, structural parameters should aid in understanding the mechanisms of carrier peptide translocation of cargo molecules across cellular membranes. Here, we have labeled Gly^{10}, Phe^{19}, Ala^{26}, and Val^{29} in the hCT(9−32) sequence and report structural and dynamical parameters for these sites.

EXPERIMENTAL PROCEDURES

Materials. The lipids 1-palmitoyl-2-oleoyl-*sn*-glycero-3-phosphocholine (POPC), 1-palmitoyl-d_{31}-2-oleoyl-*sn*-glycero-3-phosphocholine (POPC-d_{31}), 1-palmitoyl-2-oleoyl-*sn*-glycero-3-phosphoethanolamine (POPE), 1-palmitoyl-2-oleoyl-*sn*-glycero-3-[phospho-*rac*-(1-glycerol)] (sodium salt) (POPG), 1-palmitoyl-2-oleoyl-*sn*-glycero-3-phospho(TEMPO)choline (Tempo-PC), and 1-palmitoyl-2-stearoyl-(5-DOXYL)-*sn*-glycero-3-phosphocholine (5-Doxyl-PC) were purchased from Avanti Polar Lipids, Inc. (Alabaster, AL) and used without further purification. Uniformly ^{13}C- and ^{15}N-labeled N^{α}-Fmoc-protected amino acids were purchased from Cambridge Isotope Laboratories, Inc. (Andover, MA). N^{α}-Fmoc-protected amino acids, 2-(1*H*-benzotriazol-1-yl)-1,1,3,3-tetramethyluronium tetrafluoroborate (TBTU), 1-hydroxybenzotriazole (HOBt), and 4-(2′,4′-dimethoxyphenyl-Fmoc-aminomethyl)phenoxy (Rink amide) resin were obtained from Novabiochem (Läufelfingen, Switzerland). Further reagents and solvents were obtained from Sigma-Aldrich, Riedel-de-Haen, Merck, or Biosolve. Unlabeled hCT(9−32) was synthesized by Jena Bioscience (Jena, Germany).

Peptide Synthesis. The peptide fragment of residues 9−32 of human calcitonin with the sequence L G^{10}TYTQ DFNKF^{19} HTFPQ TA^{26}IGV^{29} GAP-NH_2 was synthesized by automated multiple solid-phase peptide synthesis (Fmoc strategy) using a robot system (Syro, MultiSynTech, Bochum, Germany). Double coupling procedures were carried out with DIC/HOBt activation, a 10-fold excess, and a coupling time of 40 min as reported previously (*13*, *14*). To introduce the uniformly ^{13}C- and ^{15}N-labeled amino acids Gly^{10}, Phe^{19}, Ala^{26}, and Val^{29}, the automated synthesis cycles were interrupted and manual double coupling steps with TBTU/HOBt activation in 2-fold excess were carried out. The peptide amide was cleaved from the polymer with 1 mL of a trifluoroacetic acid/thioanisole/thiocresol mixture (90:5:5, v/v/v) within 3 h and analyzed by RP-HPLC [linear gradient from 10 to 60% B in A over the course of 30 min (A = 0.1% TFA in water, and B = 0.08% TFA in ACN)] and matrix-assisted laser desorption ionization (MALDI) mass spectrometry. A correct mass was found at 2630.0 [as compared to the mass of 2631.3 calculated for hCT(9−32), including the mass increase of 23 mass units by the isotopic labeling], and the purity according to HPLC was >90%.

Sample Preparation. For MAS NMR measurements, aliquots of phospholipid mixtures in chloroform containing POPC, POPE, and POPG (in a 5:3:2 molar ratio) were combined with aliquots of isotopically labeled hCT(9−32) dissolved in methanol and chloroform (1:2, v/v) to obtain lipid:peptide molar ratios between 20:1 and 200:1. For relaxation measurements, 2 mol % of either Tempo-PC or 5-Doxyl-PC was added to the total lipid. All samples were dried under a stream of nitrogen, dissolved in cyclohexane, frozen in liquid nitrogen, and lyophilized under a vacuum of ∼0.1 mbar. Subsequently, the sample was rehydrated to 35 wt % by adding buffer [10 mM HEPES and 10 mM NaCl (pH 7.4)] and equilibrated by freeze−thaw cycles, stirring, and gentle centrifugation. The sample was finally transferred to 4 mm MAS rotors equipped with cylindrical Teflon inserts providing a volume of 50 μL.

For static ^{2}H and ^{31}P NMR measurements, unlabeled hCT(9−32) was used, but samples were prepared in a manner analogous to the MAS NMR samples, except that hydration was carried out with deuterium-depleted water. After equilibration, samples were filled into 5 mm glass vials and the vials sealed. All NMR experiments were carried out at 30 °C.

Static Solid-State NMR Experiments. ^{31}P NMR experiments were carried out on a Bruker DSX600 spectrometer (Bruker BioSpin, Rheinstetten, Germany), operating at a resonance frequency of 242.94 MHz for ^{31}P using a 5 mm double-resonance probe. ^{31}P NMR spectra were acquired using a Hahn echo pulse sequence with a delay between pulses of 50 μs, a 90° pulse length of 7 μs, a spectral width of 100 kHz, and a recycle delay of 1 s. Broadband ^{1}H decoupling was applied during signal acquisition.

^{2}H NMR spectra were recorded on a Bruker Avance 400 NMR spectrometer at a resonance frequency of 61.5 MHz for ^{2}H using a solids probe with a 5 mm solenoid coil. The ^{2}H NMR spectra were accumulated using the quadrupolar echo sequence and a relaxation delay of 0.5 s. The two 3 μs $\pi/2$ pulses were separated by a 60 μs delay. ^{2}H NMR spectra were depaked, and order parameters for each methylene group in the chain were determined as described in detail in ref *39*.

MAS NMR Experiments. All MAS NMR experiments were carried out on a Bruker AVANCE 750 spectrometer at resonance frequencies of 749.95 MHz for ^{1}H, 188.59 MHz for ^{13}C, and 76.01 MHz for ^{15}N. Either a double- or a triple-resonance MAS probe each equipped with a 4 mm spinning module was used.

CP MAS spectra were acquired using a ^{1}H 90° excitation pulse 4 μs in length and cross-polarization (CP) contact times of 700 μs for ^{13}C and 1 ms for ^{15}N. The radio frequency field strength for heteronuclear two-pulse phase modulation (TPPM) decoupling (*40*) was 62.5 MHz. The typical 90° pulse lengths used in the following experiments were 4 μs for ^{1}H, 5 μs for ^{13}C, and 6 μs for ^{15}N. A relaxation delay of 3 s was generally applied. If not indicated otherwise, the rotation frequency of the sample was 7 kHz. Chemical shifts were referenced with respect to external standards: the ^{13}C=O signal of ^{13}C-labeled Gly at 176.45 ppm and adamantane at 38.48 and 29.46 ppm. According to a recent study, these values are relative to TMS (*41*).

^{13}C T_1 relaxation times were measured using the CP inversion recovery pulse sequence (*42*) with 15 delays between 1 ms and 10 s and a relaxation delay of 10 s. The observed relaxation rates of ^{13}C in the presence of paramagnetic substances (R_1) are the sum of the dipolar relaxation rate ($R_{1,D}$), the relaxation rate due to the chemical shift anisotropy (CSA, $R_{1,CSA}$), and the paramagnetic relaxation rate ($R_{1,P}$) according to the equation $R_1 = R_{1,D} + R_{1,CSA} + R_{1,P}$. In the absence of paramagnetic probes, the relaxation rate R_1 equals the sum of $R_{1,D}$ and $R_{1,CSA}$. In the presence of spin-labeled phospholipid analogues, the paramagnetic relaxation rate $R_{1,P}$ was determined by subtracting the relaxation rate of the membrane system in the absence of a spin-label from the relaxation rate in the presence of the spin-labeled phospholipid as described in ref *43*.

Two-dimensional (2D) ^{13}C−^{13}C correlation spectra were obtained using a proton-driven spin diffusion (PDSD) mixing scheme (*44*) at a MAS frequency of 7 kHz. Spin diffusion periods of 100 and 800 ms were applied.

The strength of the ^{15}N−^{1}H and ^{13}C−^{1}H dipolar couplings was measured using the constant time dipolar and chemical shift (DIPSHIFT) pulse sequence (*45*−*47*). The strengths of these coupling values are crucial input parameters for the simulations that are necessary for the determination of the torsion angle ϕ (see below). They also provide information about the dynamics of the peptide that is being studied. For the DIPSHIFT experiment, ^{1}H−^{1}H homonuclear decoupling was achieved with the frequency-switched Lee−Goldburg (FSLG) sequence (*48*). The 360° ^{1}H pulses had a duration of 15.2 μs, yielding an effective decoupling field strength of 80 kHz. The MAS frequency was 4 kHz. Since the dipolar-induced signal decay is periodic with the rotor period, it was only necessary to acquire the signal over one rotor period in the indirect dimension. The one-rotor-period time domain data were fitted to yield the coupling strength of interest.

The torsion angle ϕ was determined using the HNCH pulse sequence (*47*). The samples were spun at an $\omega_r/2\pi$ rate of 3.8 kHz. A dephasing curve over one rotor period was obtained after Fourier transformation in the direct dimension only. These data were fitted to yield the torsion angle ϕ (see below).

Numerical Simulations. To determine the CSA, ^{31}P NMR spectra were simulated for different CSA values using Mathcad (Mathsoft, Inc., Cambridge, MA). Due to the spherical distribution of the lipid molecules, powder averaging was performed in 1° increments for the β Euler angle.

The time evolution under the C−H (or N−H) dipolar couplings in 2D DIPSHIFT experiments was simulated for one rotor period (*49*) using Mathcad. Simulations were performed for varying dipolar coupling strengths with powder averaging in 2° increments for the β and γ Euler angles. Other input parameters included the number of t_1 increments, the dwell time, and the spinning rate.

The time evolution under the influence of the Cα−H and N−H dipolar coupling tensors in the torsion angle measurements was simulated with a Fortran program described in ref *47*. Input parameters were the spinning rate, the number of time domain points, and the motionally averaged $\delta_{C\alpha-H}$

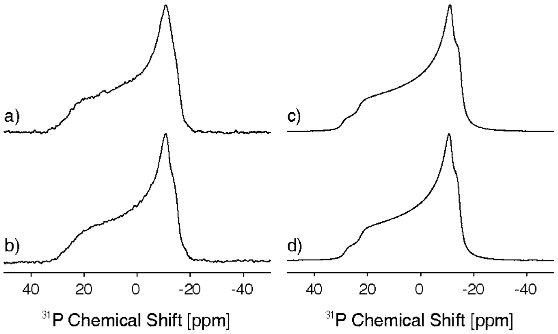

FIGURE 1: Proton-decoupled 242.9 MHz ^{31}P NMR spectra of multilamellar POPC/POPE/POPG vesicles in the absence (a) and presence (b) of 4.8 mol % hCT(9−32) at a water content of 35 wt % and 30 °C. On the right-hand side are shown numerical simulations of these spectra (c and d).

and δ_{N-H} coupling constants, determined in the DIPSHIFT experiments. Powder averaging was performed in 3° increments for all three Euler angles. The simulated curves were multiplied with an exponential decay to account for T_2 relaxation effects during the time evolution. The best agreement between simulation and experiment was determined by the smallest rmsd values.

RESULTS

Membrane Interaction of hCT(9−32). The POPC/POPE/POPG membrane mixture (5:3:2 molar ratio) was chosen to mimic the phospholipid composition of nasal epithelium (*50*). Static ^{31}P NMR spectra of the membranes in the absence and presence of hCT(9−32) are shown in Figure 1. In both cases, similar powder line shapes reveal that the samples are in a lamellar liquid-crystalline phase state. The shoulders of the peaks at higher field indicate the superposition of axially symmetric powder spectra representing the different phospholipids in the sample. The corresponding CSA values were obtained from line shape simulations. Best fits were achieved by the superposition of two simulated powder spectra at an intensity ratio of 1:1 and yielded CSA values of 44.25 and 35.25 ppm for the pure lipid sample. The higher ^{31}P CSA was attributed to POPC and the lower one to POPE and POPG (*51*). In the presence of 4.8 mol % hCT(9−32), these CSA values are reduced by 1.5 ppm each, indicating the influence of the peptide on the phospholipid headgroup.

Only a negligible influence of hCT(9−32) on lipid chain order in the membrane is detected in ^{2}H NMR experiments (data not shown). The average order parameter of POPC-d_{31} in the POPC-d_{31}/POPE/POPG mixture is reduced from 0.179 in the absence of the peptide to 0.175 in the presence of 4.8 mol % hCT(9−32), indicating that there is essentially no penetration of the peptide into the hydrophobic part of the membrane.

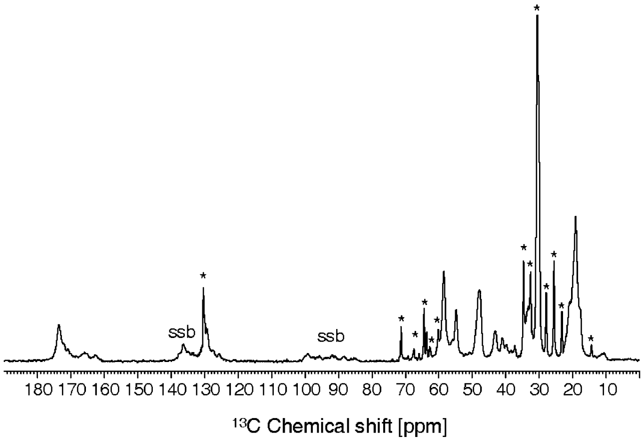

FIGURE 2: Proton-decoupled 188.6 MHz ^{13}C CP MAS spectrum of hCT(9−32) in lipid vesicles (1:50 molar ratio) at a buffer content of 35 wt % [10 mM NaCl and 10 mM Hepes (pH 7.4)]. The MAS spinning frequency was 7 kHz and the temperature 30 °C. Broad lines refer to the peptide signals. For assignment of the peptide signals, see Table 1. Lipid signals are denoted with an asterisk. ssb denotes a spinning sideband.

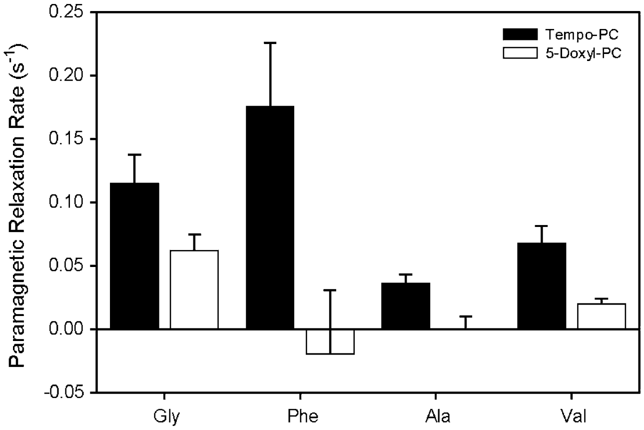

FIGURE 3: Paramagnetic relaxation rates (s^{-1}) of the Cα backbone signals of hCT(9−32) induced by paramagnetic spin probes of Tempo-PC or 5-Doxyl-PC, located in the headgroup or upper chain region of the membrane, respectively. Paramagnetic relaxation rates are a measure for the strength of the interaction between the label and the respective peptide site (*43*). The negative relaxation rate obtained for Phe Cα in the presence of 5-Doxyl-PC is due to the error in the relaxation time measurement and should be considered zero.

A typical ^{13}C CP MAS spectrum of specifically labeled hCT(9−32) in a lipid bilayer environment is shown in Figure 2. Narrow peaks correspond to lipid ^{13}C signals (line width of <0.5 ppm); broad lines refer to peptide signals. Typically, the peptide signals have a width of 1−2 ppm. Approximately the same line widths are observed in dipolar decoupled single-pulse excitation ^{13}C Bloch decay spectra (spectra not shown). In the Cα region of the spectrum (∼45−65 ppm), four peaks can be clearly identified corresponding to the four Cα signals. Before the assignment of the peptide signals and measurements about the peptide conformation are reported, relaxation experiments for determining the peptide localization with respect to the membrane are described.

In the presence of paramagnetic spin-labels, the ^{13}C relaxation rates of the peptide signals are enhanced due to interactions of the nuclear spins with the spin of the unpaired electron of the spin-label. This effect is exploited to determine the topology of hCT(9−32) in lipid bilayers by measuring T_1 relaxation times of the ^{13}Cα signals in the absence and presence of 2 mol % spin-labeled PCs. The spin-labels were attached to either the headgroup (Tempo-PC) or the C5 position (5-Doxyl-PC) of a phospholipid analogue. A reference sample with a standard composition, including 2 mol % hCT(9−32), provides the relaxation rates $R_{1,D}$ and $R_{1,CSA}$ of the peptide signals in the membrane. The paramagnetic relaxation rates $R_{1,P}$ induced by spin probes are calculated for the relaxation times in an identical sample containing 2 mol % spin-labeled PC molecules. Figure 3

Table 1: Isotropic ^{13}C Chemical Shift Values of hCT(9−32) in a Membrane Environment at Varying Peptide Concentrations Determined from ^{13}C−^{13}C Correlation Spectra at 30 °C[a]

[hCT(9−32)]		Gly^{10}	ref[b]	Phe^{19}	ref[b]	Ala^{26}	ref[b]	Val^{29}	ref[b]
0.5 mol %	^{13}Cα	43.5	44.0	54.9	54.1	48.2	49.1	58.5	58.0
	^{13}Cβ	–	–	–[c]	41.5	19.6	20.9	33.9	34.4
	^{13}CO	171.5	170.7	173.7	172.0	173.7	173.4	173.2	172.2
1 mol %	^{13}Cα	43.4	44.0	54.9	54.1	48.1	49.1	58.7	58.0
	^{13}Cβ	–	–	41.1	41.5	21.1	20.9	33.6	34.4
	^{13}CO	171.0	170.7	173.6	172.0	173.5	173.4	173.2	172.4
2 mol %	^{13}Cα	43.2	44.0	54.8	54.1	48.0	49.1	58.7	58.0
	^{13}Cβ	–	–	41.1	41.5	21.0	20.9	33.4	34.4
	^{13}CO	170.8	170.7	173.3	172.0	173.3	173.4	173.3	172.4
3.2 mol %	^{13}Cα	43.4	44.0	54.9	54.1	47.9	49.1	58.7	58.0
	^{13}Cβ	–	–	41.1	41.5	21.0	20.9	33.5	34.4
	^{13}CO	171.6	170.7	173.1	172.0	173.1	173.4	173.1	172.4

[a] Reference values represent empirical data for the β-sheet conformation (*68*). All chemical shift values are relative to TMS. [b] Chemical shift reference for random coil structures are as follows: 50.1 ppm for Ala Cα, 17.3 ppm for Ala Cβ, 174.8 ppm for Ala CO, 43.2 ppm for Gly Cα, 171.9 ppm for Gly CO, 55.2 ppm for Phe Cα, 38.2 ppm for Phe Cβ, 173.0 ppm for Phe CO, 59.1 ppm for Val Cα, 30.8 ppm for Val Cβ, and 173.1 ppm for Val CO. [c] Cross-peak on noise level.

shows the paramagnetic relaxation rates for the four Cα atoms of hCT(9−32). These rates are a measure of the proximity and the contact probability between the peptide and spin-labels (*43*). Systematically, the paramagnetic relaxation rates induced by Tempo-PC are larger than the ones induced by 5-Doxyl-PC. This indicates that the peptide is located closer to the lipid headgroups than to the acyl chains of the membrane. This is in agreement with the ^{31}P and ^{2}H NMR data indicating that hCT(9−32) does not penetrate the membrane and associates with the lipid headgroups.

hCT(9−32) Conformation in a Membrane Environment. Isotropic chemical shifts are sensitive markers for secondary structure (*52*−*54*). For instance, compared to the random coil chemical shift, a downfield shift of the ^{13}C Cα and CO signal with a simultaneous upfield shift of the Cβ signal is indicative of α-helix formation while the opposite chemical shift changes are signatures of β-sheet structures.

The isotropic chemical shifts for the four labeled amino acids of hCT(9−32) are shown in Table 1. Signals are assigned from 2D ^{13}C−^{13}C correlation spectra, provided by PDSD experiments on the samples containing either 0.5, 1.0, 2.0, or 3.2 mol % hCT(9−32). In Figure 4, a contour plot of a typical ^{13}C−^{13}C correlation spectrum is shown for 2.0 mol % hCT(9−32). A spin diffusion period of 100 ms allows the observation of correlation signals between ^{13}C spin pairs that are separated by up to three bonds, as seen for Val^{29}. The cross-peaks occur only within a labeled amino acid and allow the identification of all ^{13}C peptide signals. Thus, the lipid background at natural abundance is filtered out for off diagonal peaks. To check if longer distance correlations are present in hCT(9−32)/membrane samples, PDSD experiments with longer mixing times were performed. Correlations of longer distances could be, for instance, due to intramolecular back folding or intermolecular aggregation of the peptide. With mixing times of 800 ms, no additional cross-peaks have been observed. In principle, after spin diffusion for 800 ms, long-range ^{13}C−^{13}C correlations can be observed (*55*).

For all the lipid:peptide mixing ratios that were investigated, isotropic chemical shift values remained identical within experimental error. Independent of the amount of peptide in the membrane sample, the measured ^{13}C chemical shifts show the following trends (Table 1). The backbone carbon atoms, i.e., carbonyl groups and Cα atoms, always exhibit an upfield shift in comparison to empirical values for the random coil conformation. Simultaneously, the Cβ side chain signals are displaced to lower fields. With the exception of Phe^{19} Cα, which remains in the random coil range, all ^{13}C chemical shifts adopt values that are indicative of β-sheet structures according to empirical databases (*52*−*54*, *56*).

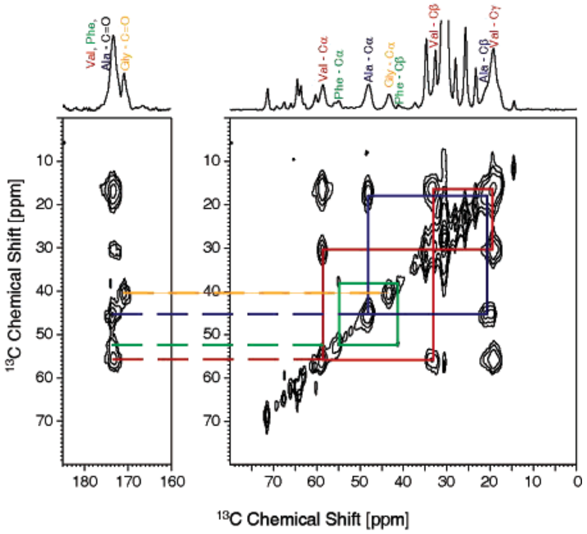

FIGURE 4: Contour plot of a ^{13}C−^{13}C correlation spectrum of 2 mol % hCT(9−32) in lipid membranes at a MAS spinning frequency of 7 kHz and 30 °C. ^{13}C−^{13}C correlations were established by a proton-driven spin diffusion period of 100 ms. Nearest neighbor correlations are highlighted. Chemical shift values and signal assignments are given in Table 1.

Referencing of chemical shifts in solid-state NMR remains challenging since no appropriate internal standards have been developed (*41*). Therefore, we have also analyzed the Cα−Cβ differences to obtain structural data independent of external referencing. Since induced Cα and Cβ chemical shifts have the opposite sign, the difference measurement provides a means of avoiding problems with absolute chemical shift referencing (*57*). At 2 mol % hCT(9−32), these differences are 27.0 ppm for Ala, 13.7 ppm for Phe, and 25.3 pmm for Val. Reference values for β-sheet structures are 28.3, 13.9, and 26.0 ppm, respectively, confirming the linear backbone conformation of hCT(9−32).

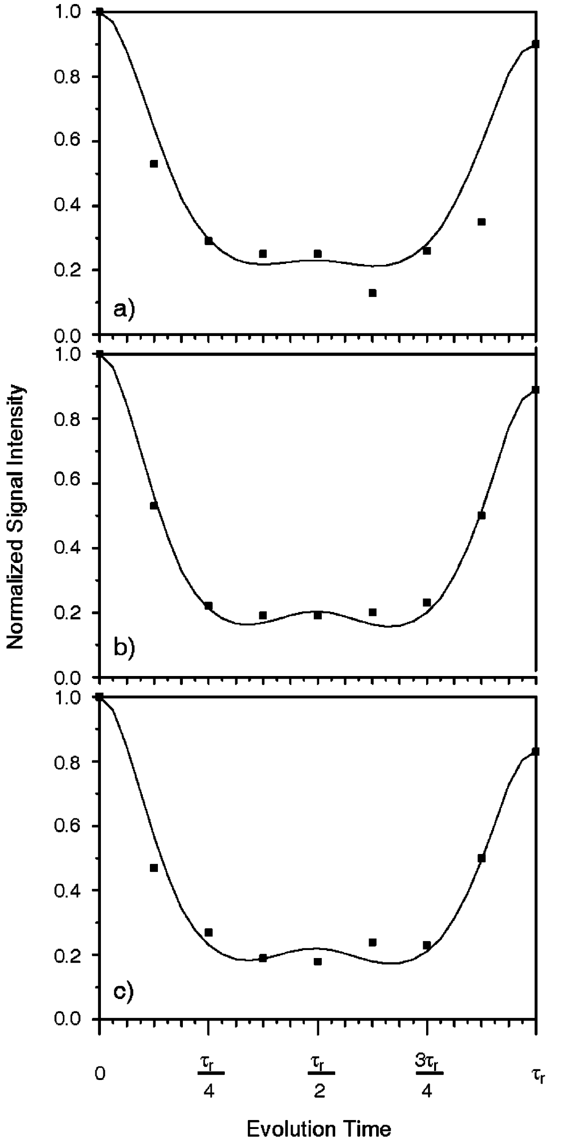

FIGURE 5: Typical dipolar dephasing curves of HNCH spectra for hCT(9−32) in a membrane environment at a peptide:lipid molar ratio of 1:50 in 35 wt % aqueous buffer [10 mM NaCl and 10 mM Hepes (pH 7.4)] (■). The acquisition time was 50 h. The different panels show Phe (a), Ala (b), and Val (c) signals. Lines represent best fit numerical simulations with ϕ torsion angles of −120° for Ala^{26} and Val^{29} and −100° or −140° for Phe^{19} (solid lines).

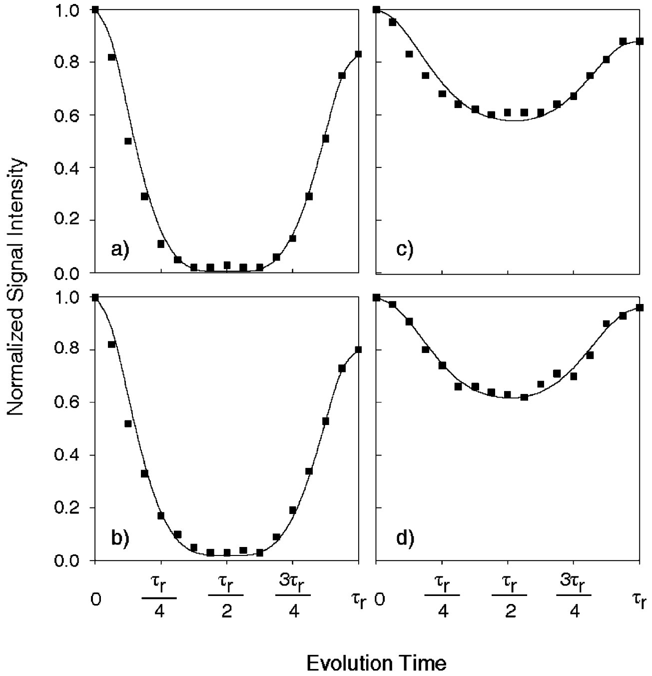

FIGURE 6: Typical ^{1}H−^{13}C and ^{1}H−^{15}N dipolar dephasing curves over one full rotor period of DIPSHIFT spectra for hCT(9−32) in a membrane environment at an $\omega_r/2\pi$ of 4 kHz and a peptide:lipid molar ratio of 1:50 (■). The different panels show Ala Cα (a), Val Cα (b), Val Cγ (c), and Phe/Val NH (d) signals. Lines represent best fit simulations. Dipolar coupling values are listed in Table 2.

To corroborate these results, the ϕ torsion angles have been measured quantitatively for the labeled amino acids in membrane-bound hCT(9−32). Figure 5 depicts typical dephasing curves of Phe^{19}, Ala^{26}, and Val^{29} of hCT(9−32) in a membrane environment recorded over one rotor period (filled symbols). The specific shape of the dephasing curves is determined by the mutual orientation of the ^{13}C−^{1}H and ^{15}N−^{1}H dipolar tensors thus containing the torsion angle information. For Gly^{10}, no unambiguous ϕ torsion angle could be determined due to the two C−H bonds in the backbone. In the case of Phe^{19}, the dephasing of the MAS signal under the influence of the dipolar tensors was slightly less pronounced than for Ala^{26} and Val^{29}. To obtain quantitative data for the torsion angle, numerical simulations have been carried out as a function of the torsion angle and compared with experimental data. The best fit (solid line) provided torsion angles of −120° for Ala^{26} and Val^{29} and −100° or −140° for Phe^{19}. Although a tolerance of ±10−15° needs to be considered, all ϕ values represent torsion angles for the β-sheet conformation in the Ramachandran diagram (*58*). These results confirm the sensitivity of the isotropic chemical shift analysis and substantiate the slight structural deviation of Phe^{19} in comparison to Ala^{26} and Val^{29}.

It should be noted that in the HNCH NMR experiment the torsion angle ϕ_H (H^{N}−N−Cα−Hα) is measured, which is related to the true backbone torsion angle ϕ (CO−N−Cα−CO) by the relationship $\phi_H = \phi - 60°$ for L-amino acids. Each simulation corresponds to two ϕ angles since the NMR experiment determines $\pm\phi_H$. The positive ϕ angle was corrected by 360° to yield the structurally relevant negative value of ϕ.

hCT(9−32) Dynamics in a Membrane Environment. To obtain dynamics information for the peptide in a lipid bilayer environment, 2D DIPSHIFT experiments were carried out to determine dipolar coupling values of the labeled amino acid residues. Since molecular motions partially average dipolar coupling values, they provide order parameters of the amplitude of the motions of the CH bond vectors; the smaller the dipolar couplings, the larger the motional amplitude. Further, the true magnitude of the scaled dipolar ^{13}C−^{1}H and ^{15}N−^{1}H couplings was used for precise simulations to calculate the ϕ torsion angles from HNCH experiments as described above.

Figure 6 depicts typical ^{13}C−^{1}H and ^{15}N−^{1}H dipolar evolution curves for the different carbon sites in the labeled amino acids of hCT(9−32). The magnitude of the dephasing corresponds to the strength of the dipolar coupling; the more dephasing, the higher the coupling value. The dephasing due to the dipolar interaction is less pronounced for the side chain signals than for ^{13}Cα−^{1}H signals. Quantitative values for the dipolar coupling strength are listed in Table 2. From these

Table 2: $^1H-^{13}C$ and $^1H-^{15}N$ Dipolar Couplings and CH Order Parameters for hCT(9−32) in a Membrane Environment at a Peptide:Lipid Molar Ratio of 1:50 at 30 °C

		$\bar{\delta}$ (kHz)	S_{CH}			$\bar{\delta}$ (kHz)	S_{CH}
Gly^{10}	Cα	10.4	0.64	Ala^{26}	Cα	11.2	0.82
	NH	4.9	–		NH	4.9	–
Phe^{19}	Cα	9.3	0.68	Val^{29}	Cα	10.9	0.80
	Cβ	8.4	0.52		Cγ	5.2	0.23
	NH	5.1	–		NH	5.1	–

motionally averaged dipolar coupling values, the molecular order parameters of the CH bonds (S_{CH}) can be calculated according to the relationship $S_{CH} = \bar{\delta}_{CH}/\delta_{CH}$, where $\bar{\delta}_{CH}$ is the motionally averaged and δ_{CH} the full dipolar coupling. Rigid limit values were obtained from measurements of crystalline amino acids as reference values for the full dipolar coupling: CH (Ala, 13.7 kHz), CH_2 (Gly, 16.3 kHz), and CH_3 (Ala, 22.8 kHz) groups (*33*).

Comparison of the order parameters of hCT(9−32) to those of other membrane-bound peptides adopting oligomeric β-sheet structure (*33*) illustrates the generally higher mobility of the carrier peptide. This is particularly true for the side chains, where significantly reduced order is obtained for all signals (S_{CH} between 0.23 and 0.52). But backbone Cα order parameters of ∼0.6−0.8 also indicate less rigidity than that assumed for oligomeric β-sheet structures stabilized by hydrogen bonding. Especially Gly^{10} and Phe^{19} show a very low order parameter for Cα.

DISCUSSION

There is a considerable controversy about the structure of hCT and its fragments in membrane and membrane-like environments. This is largely due to differences in the lipid and detergent systems as well as in the methods that have been employed to study hCT and its C-terminal fragment. In general, membrane-mimicking environments such as SDS micelles or solvents with low dielectric constants do not represent the complicated molecular nature of a lipid membrane and its lipid water interface very well. Therefore, the intention of this current study was to study hCT(9−32) in a true bilayer membrane environment and obtain quantitative structural data by solid-state NMR spectroscopy.

Interaction of hCT(9−32) with Lipid Membranes. Surprisingly, very little interaction between hCT(9−32) and lipid membranes has been observed in our study. Some influence of hCT(9−32) on the lipid headgroup region was detected by ^{31}P NMR. The observed decrease in the chemical shift anisotropy of the lipid phosphate spectra is indicative of a change in the average headgroup orientation induced by interactions with hCT(9−32) (*59*). However, the observed effects are rather small even at relatively high peptide concentrations.

Virtually no influence of hCT(9−32) on the lipid acyl chain order parameter is detected by ^2H NMR, suggesting that the peptide does not penetrate the lipid membrane. This is in agreement with previous monolayer studies in which a change in surface pressure due to adsorption of the peptide at physiologically relevant surface pressures was not observed (*27*). This prompts the question of how hCT(9−32) can translocate across the cellular membrane if there are only minimal interactions between the peptide and bilayer. One possibility could be that hCT(9−32) forms a (multimeric) α-helical or β-barrel-like transmembrane segment in the membrane. These structures do not necessarily influence lipid chain order and headgroup orientation much (*60*). Therefore, we investigated paramagnetic relaxation rates of four hCT(9−32) backbone positions induced by lipid-attached spin-labels. The paramagnetic relaxation rates induced by lipids containing a headgroup spin-label are larger than those induced by lipids with the spin-label in the acyl chain region. Such data are consistent with a surface-associated topology of hCT(9−32), while a transmembrane structure of hCT can clearly be excluded from the measurements of this study.

This at first sight surprising topology of the carrier peptide is also in agreement with hydrophobicity calculations. According to the Wimley White hydrophobicity scale (*61*), there is no propensity of the hCT(9−32) peptide for the membrane. The free energy of transferring the peptide from an aqueous environment to the membrane is slightly positive ($\Delta G = 0.67$ kcal/mol) and thus unfavorable for membrane insertion. A favorable free energy of membrane partitioning from the aqueous phase is, however, found for the N-terminal segment of hCT(9−32), i.e., amino acids 9−22, which contain several highly hydrophobic residues (three Phe residues, one Tyr, and one Leu). This region has been suggested to form an amphipathic α-helix that interacts with the membrane (*21*). In our studies, the helical structure of this segment could not be confirmed (see below). We also did not find a preferential membrane interaction of this peptide segment as probed for Gly^{10} and Phe^{19}. The C-terminus of the peptide, formerly hypothesized to be embedded in the membrane (*7*), shows the same surface topology as measured for Ala^{26} and Val^{29}. Such a surface localization seems to be a common feature of carrier peptides as many of them are not sufficiently hydrophobic to deeply penetrate the membrane (*15*). Since hCT(9−32) contains only one negative and two positive charges, electrostatic interactions between the peptide and negatively charged membranes do not contribute significant binding energy, either. Thus, we conclude that hCT(9−32) is loosely associated with the phospholipid headgroups at the membrane surface.

Structure of Membrane-Associated hCT(9−32). Quantitative measurements of isotropic chemical shifts and torsion angles for Gly^{10}, Ala^{26}, and Val^{29} indicate a largely β-sheet-like structure for the membrane-associated peptide. For Phe^{19}, the structural parameters are somewhat inconclusive (see below). The important question of whether this structure is monomeric or multimeric arises.

Though most of the determined structural parameters for the hCT(9−32) sequence agree with a β-sheet-like structure, there is no evidence that oligomeric intermolecular β-sheets with a hydrogen bond-stabilized structure are formed since fibril formation has been observed for full-length hCT (*18, 62, 63*).

Several experimental findings argue against such structural arrangements in our system. First, there is no change in the peptide structure as a function of the lipid:peptide ratio. Even at a very high dilution of one peptide per 200 lipid molecules, the isotropic chemical shifts remain largely unchanged (see Table 1). If aggregation had occurred, structural changes would have likely occurred during the aggregation process (*33*). Second, the high mobility of hCT(9−32) in the membrane environment with large amplitude motions does

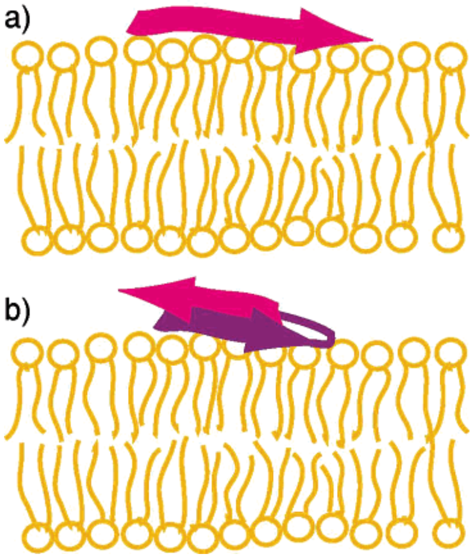

FIGURE 7: Structural models that are consistent with the structural constraints obtained from solid-state NMR experiments with hCT(9−32) in a membrane environment: (a) linear backbone conformation and (b) intramolecular antiparallel β-sheet-like structure of membrane-associated hCT(9−32). Both structures are monomeric and characterized by a high degree of molecular dynamics with large amplitude motions.

not support a multimeric arrangement of the peptide with intermolecular hydrogen bonds. Especially for the hydrogen-bonded peptide backbone in an oligomeric β-sheet structure, much higher order parameters have been observed (*33*). Third, the finding that both ^{13}C CP MAS and dipolar decoupled direct excited ^{13}C MAS spectra yield the same line widths for the peptide signals also suggests that no fibrillation of the hCT(9−32) peptides has occurred. In a recent solid-state NMR study on full-length hCT, narrow lines (∼1 ppm) have been detected for monomeric hCT (measured by Bloch decay spectra) and very broad lines (∼5 ppm and more) for hCT fibrils measured by CP MAS (*64*). In our system, both spectra yield approximately the same line widths, suggesting that no oligomerization has taken place. Fourth, there are no long-range correlations between the labeled amino acids measured at long spin diffusion periods. Due to dipolar truncation effects and the relatively high mobility of the peptide backbone, it is, however, unlikely that long-range cross-peaks can be observed in these measurements. Therefore, structural conclusions should not be made on the basis of missing cross-peaks under these circumstances.

With this limited set of data, two monomeric structural models of hCT(9−32) in a membrane environment can be determined (Figure 7). First, hCT(9−32) assumes an extended structure with β-sheet-like torsion angles on the membrane surface. Since, by definition, β-sheets are stabilized by intersheet hydrogen bonds, we refer to this structure as a linear backbone conformation. Although only four of the 24 amino acids have been structurally characterized in this study, it is rather unlikely that the amino acids between these labels show different secondary structures due to the uniformity of the observed structural parameters.

Second, back folding within the peptide strand allows the formation of an antiparallel β-sheet connected by a β-turn, for instance, as observed for amyloid peptides (*65, 66*). Such a structure is motivated from the deviations of the β-sheet geometry for Phe^{19}. The anomalies in the structure of this residue could indicate that the Phe^{19} side chain is inserted into the membrane, which has a profound impact on the structure of the peptide. However, more data are needed to support this structure, which, at the moment, is rather speculative.

In summary, we propose two structural models of hCT(9−32) in a membrane environment that are characterized by a linear or back-folded backbone conformation. These structures are relatively mobile on the fast time scale (typically correlation times of nanoseconds). Only weak interactions of the peptide with the membrane occur, suggesting a surface localization of hCT(9−32) on the lipid membrane.

What Are the Implications from Such a Structural Model for the Internalization Process of the Carrier Peptide? Several mechanisms of the internalization of carrier peptides into cells have been discussed recently in the literature. Apparently, highly positively charged cell-penetrating peptides have the ability to associate with the negatively charged membrane surface and are capable of locally inverting the surface charge of the membrane. Then, these peptides are internalized by the movement across the membrane following the membrane potential of the cell (*15*). An alternative mechanism of peptide internalization involves the protein machinery of the cell by endocytosis.

For hCT(9−32), which carries only one positive net charge, an electrostatic mechanism like that for penetratin is unlikely. Rather, an endocytic pathway of membrane internalization has been suggested. This conclusion is based mainly on the fact that a much weaker internalization occurs at 4 °C, where the energetically driven processes of the cell are mainly shut off (*67*). However, potent cargo internalization has been observed at physiological temperature.

Peptides with translocating abilities are described not only as carrier peptides but also as cell-penetrating peptides, although a recent reevaluation of the cellular internalization mechanism of these peptides generally suggests the involvement of endocytosis instead of membrane penetration (*3*). Consistently, this study implies similar circumstances for the cellular uptake of hCT(9−32) since its interactions with the membrane are very weak. Virtually no influence of hCT(9−32) on the lipid chain order parameters has been observed. However, some interactions with the headgroup region confirm that hCT(9−32) is associated with the lipid membrane. We note that the model membranes that have been used to study the hCT(9−32)−membrane interactions are by far not as complicated and diverse as real cell membranes for which the internalization of hCT has been demonstrated. Other components such as membrane proteins, glycolipids, and cholesterol may play the decisive role in that process. It is tempting to speculate that the location of hCT(9−32) near the membrane surface may trigger a range of interactions with membrane proteins, for example, thus providing the signal for the cell to activate the endocytosis mechanisms responsible for the internalization of hCT(9−32) and its cargo molecules.

ACKNOWLEDGMENT

We thank Frau R. Reppich for recording the mass spectra.

REFERENCES

1. Krauss, U., and Beck-Sickinger, A. (2002) Carrier peptides are promising tools for a broad range of applications, in *Membrane interacting proteins and peptides* (Heitz, F., Ed.) pp 25−42, Research Signpost, Trivandrum.
2. Lindgren, M., Hallbrink, M., Prochiantz, A., and Langel, U. (2000) Cell-penetrating peptides, *Trends Pharmacol. Sci. 21*, 99−103.
3. Richard, J. P., Melikov, K., Vives, E., Ramos, C., Verbeure, B., Gait, M. J., Chernomordik, L. V., and Lebleu, B. (2003) Cell-penetrating peptides. A reevaluation of the mechanism of cellular uptake, *J. Biol. Chem. 278*, 585−590.
4. Derossi, D., Chassaing, G., and Prochiantz, A. (1998) Trojan peptides: the penetratin system for intracellular delivery, *Trends Cell Biol. 8*, 84−87.
5. Morris, M. C., Vidal, P., Chaloin, L., Heitz, F., and Divita, G. (1997) A new peptide vector for efficient delivery of oligonucleotides into mammalian cells, *Nucleic Acids Res. 25*, 2730−2736.
6. Pooga, M., Hallbrink, M., Zorko, M., and Langel, U. (1998) Cell penetration by transportan, *FASEB J. 12*, 67−77.
7. Schmidt, M. C., Rothen-Rutishauser, B., Rist, B., Beck-Sickinger, A., Wunderli-Allenspach, H., Rubas, W., Sadee, W., and Merkle, H. P. (1998) Translocation of human calcitonin in respiratory nasal epithelium is associated with self-assembly in lipid membrane, *Biochemistry 37*, 16582−16590.
8. Lang, S., Rothen-Rutishauser, B., Perriard, J. C., Schmidt, M. C., and Merkle, H. P. (1998) Permeation and pathways of human calcitonin (hCT) across excised bovine nasal mucosa, *Peptides 19*, 599−607.
9. Pontiroli, A. E., Alberetto, M., and Pozza, G. (1985) Intranasal calcitonin and plasma calcium concentrations in normal subjects, *Br. Med. J. 290*, 1390−1391.
10. Silverman, S. L. (1997) Calcitonin, *Am. J. Med. Sci. 313*, 13−16.
11. Stroop, S. D., Nakamuta, H., Kuestner, R. E., Moore, E. E., and Epand, R. M. (1996) Determinants for calcitonin analog interaction with the calcitonin receptor N-terminus and transmembrane-loop regions, *Endocrinology 137*, 4752−4756.
12. Machova, Z., Muhle, C., Krauss, U., Trehin, R., Koch, A., Merkle, H. P., and Beck-Sickinger, A. G. (2002) Cellular internalization of enhanced green fluorescent protein ligated to a human calcitonin-based carrier peptide, *ChemBioChem 3*, 672−677.
13. Krauss, U., Kratz, F., and Beck-Sickinger, A. G. (2003) Novel daunorubicin-carrier peptide conjugates derived from human calcitonin segments, *J. Mol. Recognit. 16*, 280−287.
14. Krauss, U., Muller, M., Stahl, M., and Beck-Sickinger, A. G. (2004) In vitro gene delivery by a novel human calcitonin (hCT)-derived carrier peptide, *Bioorg. Med. Chem. Lett. 14*, 51−54.
15. Binder, H., and Lindblom, G. (2003) Charge-dependent translocation of the Trojan peptide penetratin across lipid membranes, *Biophys. J. 85*, 982−995.
16. Bauer, H. H., Muller, M., Goette, J., Merkle, H. P., and Fringeli, U. P. (1994) Interfacial adsorption and aggregation associated changes in secondary structure of human calcitonin monitored by ATR-FTIR spectroscopy, *Biochemistry 33*, 12276−12282.
17. Kamihira, M., Oshiro, Y., Tuzi, S., Nosaka, A. Y., Saito, H., and Naito, A. (2003) Effect of electrostatic interaction on fibril formation of human calcitonin as studied by high-resolution solid state ^{13}C NMR, *J. Biol. Chem. 278*, 2859−2865.
18. Arvinte, T., Cudd, A., and Drake, A. F. (1993) The structure and mechanism of formation of human calcitonin fibrils, *J. Biol. Chem. 268*, 6415−6422.
19. Arvinte, T., and Drake, A. F. (1993) Comparative study of human and salmon calcitonin secondary structure in solutions with low dielectric constants, *J. Biol. Chem. 268*, 6408−6414.
20. Epand, R. M., Epand, R. F., and Orlowski, R. C. (1985) Presence of an amphipathic helical segment and its relationship to biological potency of calcitonin analogs, *Int. J. Pept. Protein Res. 25*, 105−111.
21. Epand, R. M., Epand, R. F., Orlowski, R. C., Schlueter, R. J., Boni, L. T., and Hui, S. W. (1983) Amphipathic helix and its relationship to the interaction of calcitonin with phospholipids, *Biochemistry 22*, 5074−5084.
22. Hashimoto, Y., Toma, K., Nishikido, J., Yamamoto, K., Haneda, K., Inazu, T., Valentine, K. G., and Opella, S. J. (1999) Effects of glycosylation on the structure and dynamics of eel calcitonin in micelles and lipid bilayers determined by nuclear magnetic resonance spectroscopy, *Biochemistry 38*, 8377−8384.
23. Motta, A., Pastore, A., Goud, N. A., and Castiglione Morelli, M. A. (1991) Solution conformation of salmon calcitonin in sodium dodecyl sulfate micelles as determined by two-dimensional NMR and distance geometry calculations, *Biochemistry 30*, 10444−10450.
24. Motta, A., Andreotti, G., Amodeo, P., Strazzullo, G., and Castiglione Morelli, M. A. (1998) Solution structure of human calcitonin in membrane-mimetic environment: the role of the amphipathic helix, *Proteins 32*, 314−323.
25. Motta, A., Temussi, P. A., Wunsch, E., and Bovermann, G. (1991) A ^{1}H NMR study of human calcitonin in solution, *Biochemistry 30*, 2364−2371.
26. Epand, R. M., Epand, R. F., and Orlowski, R. C. (1988) Biologically active calcitonin analogs which have minimal interactions with phospholipids, *Biochem. Biophys. Res. Commun. 152*, 203−207.
27. Wagner, K., Van Mau, N., Boichot, S., Kajava, A. V., Krauss, U., Le Grimellec, C., Beck-Sickinger, A., and Heitz, F. (2004) Interactions of human calcitonin fragment 9−32 with phospholipids: a monolayer study, *Biophys. J. 87*, 386−395.
28. Marsh, D. (1996) Lateral pressure in membranes, *Biochim. Biophys. Acta 1286*, 183−223.
29. Stejskal, E. O., and Schaefer, J. (1976) Carbon-13 nuclear magnetic resonance of polymers spinning at the magic angle, *J. Am. Chem. Soc. 98*, 1031−1032.
30. Torres, J., Stevens, T. J., and Samso, M. (2003) Membrane proteins: the ‘Wild West’ of structural biology, *Trends Biochem. Sci. 28*, 137−144.
31. Luca, S., White, J. F., Sohal, A. K., Filippov, D. V., van Boom, J. H., Grisshammer, R., and Baldus, M. (2003) The conformation of neurotensin bound to its G protein-coupled receptor, *Proc. Natl. Acad. Sci. U.S.A. 100*, 10706−10711.
32. Ketchem, R. R., Hu, W., and Cross, T. A. (1993) High-resolution conformation of gramicidin A in a lipid bilayer by solid-state NMR, *Science 261*, 1457−1460.
33. Barré, P., Zschörnig, O., Arnold, K., and Huster, D. (2003) Structural and Dynamical Changes of the Bindin B18 Peptide upon Binding to Lipid Membranes. A Solid-State NMR Study, *Biochemistry 42*, 8377−8386.
34. Lam, Y. H., Wassall, S. R., Morton, C. J., Smith, R., and Separovic, F. (2001) Solid-state NMR structure determination of melittin in a lipid environment, *Biophys. J. 81*, 2752−2761.
35. Yang, J., Gabrys, C. M., and Weliky, D. P. (2001) Solid-state nuclear magnetic resonance evidence for an extended β strand conformation of the membrane-bound HIV-1 fusion peptide, *Biochemistry 40*, 8126−8137.
36. Hirsh, D. J., Hammer, J., Maloy, W. L., Blazyk, J., and Schaefer, J. (1996) Secondary structure and location of a magainin analogue in synthetic phospholipid bilayers, *Biochemistry 35*, 12733−12741.
37. Zeri, A. C., Mesleh, M. F., Nevzorov, A. A., and Opella, S. J. (2003) Structure of the coat protein in fd filamentous bacteriophage particles determined by solid-state NMR spectroscopy, *Proc. Natl. Acad. Sci. U.S.A. 100*, 6458−6463.
38. Kaiser, E., Colescott, R. L., Bossinger, C. D., and Cook, P. I. (1970) Color test for detection of free terminal amino groups in the solid-phase synthesis of peptides, *Anal. Biochem. 34*, 595−598.
39. Huster, D., Arnold, K., and Gawrisch, K. (1998) Influence of docosahexaenoic acid and cholesterol on lateral lipid organization in phospholipid membranes, *Biochemistry 37*, 17299−17308.
40. Bennett, A. E., Rienstra, C. M., Auger, M., Lakshmi, K. V., and Griffin, R. G. (1995) Heteronuclear decoupling in rotating solids, *J. Chem. Phys. 103*, 6951−6958.
41. Morcombe, C. R., and Zilm, K. W. (2003) Chemical shift referencing in MAS solid state NMR, *J. Magn. Reson. 162*, 479−486.
42. Torchia, D. A., and Szabo, A. (1982) Spin−lattice relaxation in solids, *J. Magn. Reson. 49*, 107−121.
43. Vogel, A., Scheidt, H. A., and Huster, D. (2003) The distribution of lipid attached EPR probes in bilayers. Application to membrane protein topology, *Biophys. J. 85*, 1691−1701.
44. Szeverenyi, N. M., Sullivan, M. J., and Maciel, G. E. (1982) Observation of spin exchange by two-dimensional Fourier transform ^{13}C cross polarization magic-angle spinning, *J. Magn. Reson. 47*, 462−475.
45. Munowitz, M. G., Griffin, R. G., Bodenhausen, G., and Huang, T. H. (1981) Two-dimensional rotational spin−echo nuclear magnetic resonance in solids: correlation of chemical shift and dipolar interactions, *J. Am. Chem. Soc. 103*, 2529−2533.

46. Schaefer, J., Stejskal, E. O., McKay, R. A., and Dixon, W. T. (1983) Dipolar rotational-echo ^{13}C-NMR of polymers, *J. Magn. Reson. 52*, 123−129.
47. Hong, M., Gross, J. D., and Griffin, R. G. (1997) Site-resolved determination of peptide torsion angle Φ from relative orientations of backbone N−H and C−H bonds by solid-state NMR, *J. Phys. Chem. 101*, 5869−5874.
48. Bielecki, A., Kolbert, A. C., and Levitt, M. H. (1989) Frequency-switched pulse sequences: homonuclear decoupling and dilute spin NMR in solids, *Chem. Phys. Lett. 155*, 341−345.
49. Schmidt-Rohr, K., and Spiess, H. W. (1994) *Multidimensional solid-state NMR and polymers*, Academic Press, San Diego.
50. Russell, Y., Evans, P., and Dodd, G. H. (1989) Characterization of the total lipid and fatty acid composition of rat olfactory mucosa, *J. Lipid Res. 30*, 877−884.
51. Huster, D., Yao, X., Jakes, K. S., and Hong, M. (2002) Conformational changes of colicin Ia channel-forming domain upon membrane binding: a solid-state NMR study, *Biochim. Biophys. Acta 1561*, 159−170.
52. Wishart, D. S., Sykes, B. D., and Richards, F. M. (1991) Relationship between nuclear magnetic resonance chemical shift and protein secondary structure, *J. Mol. Biol. 222*, 311−333.
53. Wishart, D. S., and Sykes, B. D. (1994) Chemical shifts as a tool for structure determination, *Methods Enzymol. 239*, 363−392.
54. Spera, S., and Bax, A. (1991) Empirical correlation between protein backbone conformation and Cα and Cβ ^{13}C nuclear magnetic resonance chemical shifts, *J. Am. Chem. Soc. 113*, 5490−5492.
55. Castellani, F., van Rossum, B., Diehl, A., Schubert, M., Rehbein, K., and Oschkinat, H. (2002) Structure of a protein determined by solid-state magic-angle-spinning NMR spectroscopy, *Nature 420*, 98−102.
56. Saito, H., Tuzi, S., and Naito, A. (2001) Empirical versus nonempirical evaluation of secondary structure of fibrous and membrane proteins by solid-state NMR: a practical approach, *Annu. Rep. NMR Spectrosc. 38*, 79−121.
57. Luca, S., Filippov, D. V., van Boom, J. H., Oschkinat, H., de Groot, H. J., and Baldus, M. (2001) Secondary chemical shifts in immobilized peptides and proteins: a qualitative basis for structure refinement under magic angle spinning, *J. Biomol. NMR 20*, 325−331.
58. Creighton, T. E. (1993) *Proteins. Structures and molecular properties*, W. H. Freeman and Company, New York.
59. Scherer, P. G., and Seelig, J. (1989) Electric charge effects on phospholipid headgroups. Phosphatidylcholine in mixtures with cationic and anionic amphiphiles, *Biochemistry 28*, 7720−7728.
60. de Planque, M. R., Greathouse, D. V., Koeppe, R. E., II, Schafer, H., Marsh, D., and Killian, J. A. (1998) Influence of lipid/peptide hydrophobic mismatch on the thickness of diacylphosphatidylcholine bilayers. A ^{2}H NMR and ESR study using designed transmembrane α-helical peptides and gramicidin A, *Biochemistry 37*, 9333−9345.
61. Wimley, W. C., and White, S. H. (1996) Experimentally determined hydrophobicity scale for proteins at membrane interfaces, *Nat. Struct. Biol. 3*, 842−848.
62. Naito, A., Kamihira, M., Inoue, R., and Saito, H. (2004) Structural diversity of amyloid fibril formed in human calcitonin as revealed by site-directed ^{13}C solid-state NMR spectroscopy, *Magn. Reson. Chem. 42*, 247−257.
63. Kanaori, K., and Nosaka, A. Y. (1995) Study of human calcitonin fibrillation by proton nuclear magnetic resonance spectroscopy, *Biochemistry 34*, 12138−12143.
64. Kamihira, M., Naito, A., Tuzi, S., Nosaka, A. Y., and Saito, H. (2000) Conformational transitions and fibrillation mechanism of human calcitonin as studied by high-resolution solid-state ^{13}C NMR, *Protein Sci. 9*, 867−877.
65. Tycko, R. (2003) Insights into the amyloid folding problem from solid-state NMR, *Biochemistry 42*, 3151−3159.
66. Petkova, A. T., Ishii, Y., Balbach, J. J., Antzutkin, O. N., Leapman, R. D., Delaglio, F., and Tycko, R. (2002) A structural model for Alzheimer's β-amyloid fibrils based on experimental constraints from solid-state NMR, *Proc. Natl. Acad. Sci. U.S.A. 99*, 16742−16747.
67. Trehin, R., Krauss, U., Muff, R., Meinecke, M., Beck-Sickinger, A. G., and Merkle, H. P. (2004) Cellular internalization of human calcitonin derived peptides in MDCK monolayers: a comparative study with Tat(47−57) and penetratin(43−58), *Pharm. Res. 21*, 33−42.
68. http://www.bmrb.wisc.edu/index.html.

BI049181Y